The Effects of Climate Change on Seasonal Snowpack and the Hydrology of the Northeastern and Upper Midwest United States

ELEONORA M. C. DEMARIA[a]

Northeast Climate Science Center, University of Massachusetts, Amherst, Massachusetts

JOSHUA K. ROUNDY

Department of Civil, Environmental, and Architectural Engineering, University of Kansas, Lawrence, Kansas

SUNGWOOK WI

Department of Civil and Environmental Engineering, University of Massachusetts, Amherst, Massachusetts

RICHARD N. PALMER

Northeast Climate Science Center, and Department of Civil and Environmental Engineering, University of Massachusetts, Amherst, Massachusetts

(Manuscript received 4 September 2015, in final form 7 June 2016)

ABSTRACT

The potential effects of climate change on the snowpack of the northeastern and upper Midwest United States are assessed using statistically downscaled climate projections from an ensemble of 10 climate models and a macroscale hydrological model. Climate simulations for the region indicate warmer-than-normal temperatures and wetter conditions for the snow season (November–April) during the twenty-first century. However, despite projected increases in seasonal precipitation, statistically significant negative trends in snow water equivalent (SWE) are found for the region. Snow cover is likely to migrate northward in the future as a result of warmer-than-present air temperatures, with higher loss rates in northern latitudes and at high elevation. Decreases in future (2041–95) snow cover in early spring will likely affect the timing of maximum spring peak streamflow, with earlier peaks predicted in more than 80% of the 124 basins studied.

1. Introduction

Long-term fluctuations in snowpack have important implications for the sustainability of natural ecosystems in snow-dominated environments. Warmer air temperatures, linked to anthropogenic activities, have triggered significant reductions in snow cover extent over high northern latitudes during the last 100 years, in particular during the spring season when snow melting processes initiate (Brown 2000; Brown and Robinson 2011; Derksen and Brown 2012; Dyer and Mote 2006). In North America and Eurasia, snow cover has experienced an approximate 11% decrease in March–April during the twentieth century, with accelerated rates of decrease since 1970. The average rate of decrease has been reported to be ~0.8 million km^2 per decade, which roughly corresponds to a loss of one-third the area of Canada (Brown and Robinson 2011). Observations indicate that the onset of the snow season has shifted toward later dates in North America (Choi et al. 2010; Peng et al. 2013), and that late spring snow coverage has been at its lowest since the year 1967 when satellite estimates became available (Derksen and Brown 2012), with most of the decline explained by a combination of

[a] Current affiliation: Southwest Watershed Research Center, USDA-ARS, Tucson, Arizona.

Corresponding author address: Eleonora M.C. Demaria, Northeast Climate Science Center, 42C Marston Hall, Natural Resources Road, Amherst, MA, 01003-9293.
E-mail: eleonora.demaria@ars.usda.gov

DOI: 10.1175/JCLI-D-15-0632.1

natural and anthropogenic forces but not by natural forcing alone (Rupp et al. 2013).

General circulation model (GCM) climate projections for the twenty-first century indicate significant continued declining trends in snow water equivalent (SWE) and snowfall, including an early retreat of the last day of spring snowfall (Pierce and Cayan 2013). Across northeastern North America, an ensemble of 15 climate models predicts average decreases in mean winter–spring SWE (November–May) ranging from −10 to −30 mm between the years 1971–2000 and 2070–99 (Maloney et al. 2014). Climate simulations from phase 5 of the Coupled Model Intercomparison Project (CMIP5) project declines in snowfall in spring and fall during the twenty-first century in the region (Kapnick and Delworth 2013; Krasting et al. 2013).

The U.S. northeastern and upper Midwest regions (NE-UM) are the study area of the recently created Northeast Climate Science Center. The NE-UM region encompasses the 22 U.S. states east of the 98°W meridian and north of 36°N latitude, and is inhabited by 40% of the U.S. population (~131 million people). Regional population is projected to increase 20% by the year 2050, imposing more stress on natural and socioeconomic systems. In the NE-UM, changes in snow cover are extremely important for ecosystem function as shifts in the timing and volume of spring snowmelt can be critical to aquatic species that rely on them for vital transitions in their life cycles (Comte et al. 2013; Hayhoe et al. 2007). Decreases in the length of the snow season due to warmer temperatures can affect survival mechanisms of some mammals (Mills et al. 2013), as well as bird species' geographical distribution (Crick 2004), migration patterns (Cotton 2003), and timing of egg laying (Grabowski et al. 2013).

The impact of early snowmelt, linked to a warmer climate, on water availability has been extensively documented in the western United States where water resources are essential for farming and water supply for rapidly growing western cities (Barnett et al. 2005; Pierce et al. 2008; Wi et al. 2012). Changes in the phase of precipitation from solid to liquid and early snowmelt have been observed and associated with changes in river flows during the twentieth century (Hidalgo et al. 2009). In the eastern United States, Notaro et al. (2014) projected a decline in the number of days with existing snowpack and an increase in the intensity of snowfall events using statistically downscaled CMIP3 climate model simulations as input to an empirically based snow model (SNOW-17) to generate snowfall projections for the twenty-first century.

Despite the dependence of natural ecosystems on snow for their subsistence in the NE-UM region, the projected climate-driven changes in snow depth, length of the snow season, and timing and magnitude of spring flows during the twenty-first century has not been assessed at a spatiotemporal scale that effectively aids stakeholders in their resource management decisions. To fill this need, the goal of this study is threefold: 1) to generate high-resolution projections of winter snow for the NE-UM using a physically based hydrologic model forced with statistically downscaled climate model projections, 2) to estimate the presence of monotonic linear trends and quantify changes in cold season snow, and 3) to quantify the impact of spring snowpack changes on streamflow characteristics in the region.

2. Data and methodology

a. Data and hydrological model

This study is divided into two periods, the historical period (1951–2005) and the projection period (2041–95). The purpose of the historical period is to establish the utility of the model to produce historical snowpack and streamflow estimates using observed climate forcing data. The observed forcing data includes daily observations of precipitation, maximum, and minimum temperature at a 0.125° spatial resolution from the National Land Data Assimilation System version 2.0 (NLDAS-2; Xia et al. 2012) for the period of 1980–2008 and from the Maurer et al. (2002) dataset for the period of 1950–2005. The former was used to calibrate the hydrological model, while the latter was used to temporally disaggregate (i.e., from monthly to daily) the climate model simulations due to its longer record. The projected climate forcings include precipitation and temperature from 10 GCMs (Table 1) from the World Climate Research Project (WCRP) CMIP5 (Taylor et al. 2012). The best performing GCMs for the region were selected using a modified version of the reliability ensemble average (REA) method (Dominguez et al. 2010). The REA evaluates the individual model skills to simulate the present-day climate and the convergence of future climate to the ensemble mean (Demaria et al. 2016). The projections include two gas concentration scenarios: a medium concentration trajectory [representative concentration path (RCP) 4.5] and a high concentration trajectory (RCP 8.5) (Knutti and Sedlacek 2013).

To create the high-resolution gridded climate inputs needed to force the hydrological model, downscaled monthly precipitation and maximum and minimum temperature were obtained at a 0.125° spatial resolution from the publicly available bias-corrected and spatial disaggregated (BCSD) archives available online at http://gdo-dcp.ucllnl.org/downscaled_cmip_projections (Maurer et al. 2007).

TABLE 1. Climate model names and hosting institutions used in this study. Expansions of acronyms are available online at http://www.ametsoc.org/PubsAcronymList.

	Model	Modeling center
1	BCC-CSM1.1	Beijing Climate Center, China Meteorological Administration, China
2	CCSM4	National Center of Atmospheric Research, United States
3	CESM1-BGC	Community Earth System Model contributors
4	CNRM-CM5	National Centre of Meteorological Research, France
5	CSIRO-Mk3.6.0	Commonwealth Scientific and Industrial Research Organization/Queensland Climate Change Centre of Excellence, Australia
6	FIO-ESM	The First Institute of Oceanography, School of Oceanography, China
7	GFDL-ESM2G	NOAA Geophysical Fluid Dynamics Laboratory, United States.
8	IPSL-CM5A-MR	Institut Pierre Simon Laplace, France
9	MIROC5	Atmosphere and Ocean Research Institute (The University of Tokyo), National Institute for Environmental Studies, and Japan Agency for Marine-Earth Science and Technology, Japan
10	NorESM1-m	Norwegian Climate Center, Norway

The monthly precipitation and temperature values were temporally disaggregated into daily values by randomly selecting daily time series from the observed records [for details the reader is referred to Wood et al. (2002)]. For each month of the GCM, for instance May 2035, one month is randomly drawn from the pool of observed months (e.g., September 1964) and used to disaggregate all the grid cells in the domain in order to maintain the spatial structure of the storms. First, the anomaly between the monthly mean of observed and GCM maximum and minimum temperatures is computed for each climate models. Second, this anomaly is added to the daily observations to obtain daily maximum and minimum GCM temperatures. This method has been shown to effectively reproduce extreme events and wet day frequencies at different spatial and temporal scales (Gutmann et al. 2014), and it yields a product where the monthly precipitation and temperature are generated from the GCM with the day-to-day variability that has been observed in the historical record. This might lead to discrepancies in the representation of submonthly variability, if the characteristic sequence of daily event changes in the future.

The variable infiltration capacity hydrologic model (VIC) was used to simulate daily snow fields for the historical and the projection periods. VIC is a macroscale hydrological model that represents the partitioning of incoming moisture and energy at the surface and subsurface on spatially distributed cells (Liang et al. 1994; Liang et al. 1996). Distinguishing characteristics of VIC include the subgrid-scale representation of topography, vegetation, soil moisture storage capacity, and precipitation. The snow parameterization in VIC makes it suitable for regional characterization of snow processes since it represents snow accumulation and ablation processes using a two-layer energy and mass balance approach (Andreadis et al. 2009). Each model grid cell can be partitioned into multiple snow (elevation) bands that allow representing snow processes in different topographic levels, and snow interception is also modeled if vegetation canopy is present (Storck et al. 2002). The model has been previously used as a surrogate for in situ hydroclimatic observations to investigate spatial and temporal changes in snow cover once it has been calibrated with observed streamflow (Shi et al. 2013).

The VIC model (version 4.0.6) was built based on a 0.125° spatial resolution and it was run at a daily time step with a 3-h snow model. Precipitation was assumed uniformly distributed within each grid cell whereas snow processes were represented with 10 elevation bands to better describe changes in complex terrain. Daily streamflows from 124 USGS basins part of the Geospatial Attributes of Gauges for Evaluating Streamflow (Gauges II) dataset were used to calibrate the model. The basins in this dataset have near-natural conditions (i.e., basins with no impoundments, flow diversions, or other factors that could influence natural streamflows) and long streamflow records (Falcone et al. 2010). The calibrated VIC parameters were obtained from Princeton University as described in Yuan et al. (2013) following the approach described by Troy et al. (2008). Specifically, the six most commonly targeted parameters were calibrated for the 1980–2004 period against the USGS stream gauges using the precipitation and temperature forcing from the NLDAS-2 dataset. The calibrated parameters included the infiltration parameter (b), the maximum base flow generated in the deepest layer (D_m), the fraction of D_m where nonlinear base flow begins (D_s), the fraction of maximum soil moisture where nonlinear base flow is generated (W_s), and the thickness of the second and third soil layers (D_2 and D_3, respectively). Soil was represented with three layers: the uppermost layer is 0.1 m thick whereas the thickness of the second and third layer ranges from 0.1 to 2.97 m

depending on the location. All other soil, vegetation, and snow parameters were obtained from the NLDAS dataset and set to their a priori values. A channel routing scheme was used to generate daily streamflow simulations at each basin outlet (Lohmann et al. 1998). The routing model parameters (wave velocity, diffusivity, and the impulse response function) were independently calibrated from the VIC parameters also using the shuffled complex evolutionary (SCE) algorithm (Duan et al. 1992). Once the model skill to represent the region hydrology was validated, the VIC model was run over the whole NE-UM region.

To assess the ability of the VIC model to reproduce snowpack from the meteorological forcing, the VIC simulated snow depth is compared to a gridded monthly snow depth dataset from the Meteorological Service of Canada (Brown et al. 2003). These snow fields cover the period of 1979–96 at 0.25° spatial resolution and combine snow depth observations with an empirically estimated snow depth using the precipitation from the European Centre for Medium-Range Weather Forecasts (ECMWF) model.

b. Methods

To assess the change in snowpack during the historical and projection period, the length of the snow season was determined for the region. Observed interpolated snow fields are only available at the monthly time step, so simulated daily snow fields were obtained by forcing VIC with the NLDAS-2 dataset for the period 1982–2010 (the two first years were used as model spinup). Using the maximum period of time with at least 2.54 cm (approximately 1 in.) of snow on the ground as criteria, the snow season was defined as November through April for the whole NE-UM domain.

Because of the large geographic extent of the study area, and to facilitate more meaningful comparisons, the study region was divided into four 3° latitudinal bands: 36°–39°N, 39°–42°N, 42°–45°N, and 45°–49°N. Monotonic linear trends in precipitation, temperature, and SWE were computed with the nonparametric Mann–Kendall test using the tau-based slope estimator with Sen's method (Kendall 1975; Mann 1945; Sen 1968). Trends were deemed statistically different from zero at a 95% level. Changes in snow depth with elevation were evaluated for 200-m altitudinal bands (approximately 657 ft.). Maps showing the marginal probability of occurrence of monthly mean snow depths equal or larger than 2.5, 5, 10, and 20 cm were created for the study area.

To evaluate if decreases in snow depth were linked to changes in precipitation phase (from solid to liquid), the ratios between the number of snow days and wet days (solid and liquid) were computed with Eq. (1) (Das et al. 2011; Demaria et al. 2013):

$$\text{Snow} = \begin{cases} 0 & \text{for} \quad T \geq T_r \\ P\left(\dfrac{T - T_r}{T_s - T_r}\right) & \text{for} \quad T_s < T < T_r, \\ P & \text{for} \quad T \leq T_s \end{cases} \tag{1}$$

where P is daily precipitation, T is the mean daily temperature for each grid cell, T_r is the minimum temperature at which 100% liquid rain will fall (+0.5°C), and T_s is the maximum temperature at which 100% solid precipitation will fall (−0.5°C). This model, which is the same mathematical formulation implemented in VIC, is sensitive to changes in the threshold parameters; however, based on previous studies (Andreadis et al. 2009; Das et al. 2011; Das et al. 2009) and to be consistent with the VIC model simulations, −0.5°C and +0.5°C values were used and no sensitivity analysis was performed.

To evaluate how spatially projected changes in snowpack will affect the hydrology of the region, changes in center timing (CT), defined as the day when half the annual (water year) flow volume has passed a given point (Stewart et al. 2005), were computed for each basin and each climate model. For this study the water year was defined as 1 October to 30 September following the USGS definition. All the CTs contained in each latitudinal band were averaged and the presence of trends was evaluated with the Mann–Kendall test. CT values were smoothed with an 11-yr moving average. To investigate if future changes in snow cover in the region will have an impact on spring [March–May (MAM)] peak flows, first the maximum annual peak flow and its timing were obtained for each basin and each climate model. Second, changes in the magnitude and timing of peak flows between historical and future periods were computed for each basin. The statistical significance of the changes was evaluated with the Wilcoxon nonparametric test (Wilks 2006). Changes were estimated as

$$\Delta = (X_{\text{fut}} - X_{\text{hist}})/X_{\text{hist}} \times 100, \tag{2}$$

where X represents the hydrological variable of interest, the subscript "fut" the period 2041–95, and the subscript "hist" the period 1951–2005.

3. Results

a. Validation of simulated snow fields

The VIC model has been calibrated and validated for 124 basins (Fig. 1a) in the NE-UM region. During the calibration period (1980–2004), simulated monthly streamflows showed mean Nash–Sutcliffe efficiency (NSE) values of 0.70 (±0.14), relative bias (PBIAS) values of +2.5% (±16.6%), and NSE of the logarithm of the flows

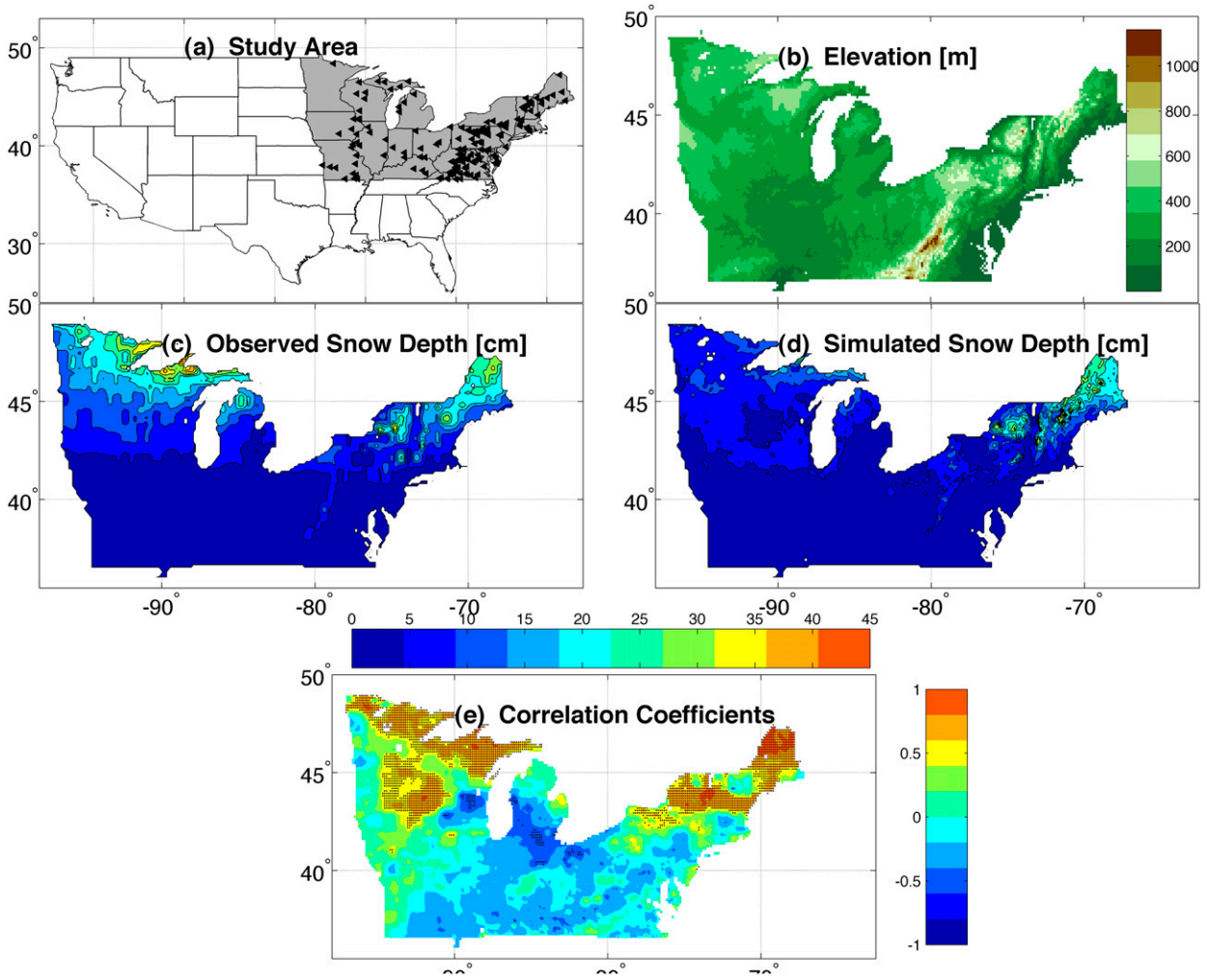

FIG. 1. (a) Location of the study area. The black triangles denote the location of the basins included in the study. (b) Topographic elevation in meters. Season average snow depth (in cm) for the winter season (November–April) for the period 1981–97 (c) observed (Brown et al. 2003) and (d) VIC observation-driven simulations. (e) Pearson correlation coefficients between seasonal averaged anomalies observed and VIC-simulated snow depth; the stippling indicates statistically significant correlations at 5% significance level.

(NSE_log) values of 0.61 (±0.27). The performance of the model deteriorates during the validation period (2005–10) with NSE and NSE_log values of 0.54 and 0.29, respectively, and negative PBIAS (−1.97). Additionally, NLDAS-2-driven VIC snow-depth simulations were compared with gridded observations from the Brown et al. (2003) dataset for the period of 1981–97. Observed snow-depth fields, available at 0.25° resolution, were regridded to a common 0.125° grid using a cubic interpolation. The winter snow climatology is characterized by a thick snowpack over high latitudes with little orographic control (Fig. 1b), as is the case in the western United States, in New England, and in the Great Lakes region where mean seasonal values reach 50 cm. Figures 1c and 1d show the November–March averaged snow depth for observations and VIC simulations, respectively. VIC-simulated snow-depth fields replicate a reasonably realistic spatial pattern when compared to the observed fields. In the northwestern part of the domain, VIC simulations generally underestimate snow depth. However, along the eastern side of the domain, VIC simulations accurately capture both spatial distribution and magnitude of snow. Pearson correlation coefficients between seasonal averaged anomalies observations and VIC simulations show strong agreement in the northern part of the study area with statistically significant correlation values larger than 0.5 (Fig. 1e). These prove the ability of VIC to reproduce the snow fields in a reasonable manner and augment the current literature in which the VIC model was satisfactorily used to generate snow products in the United States (Das et al. 2009; Pierce and Cayan 2013; Shi et al. 2013). One possibility causing the discrepancies between observations and simulations, in particular at higher

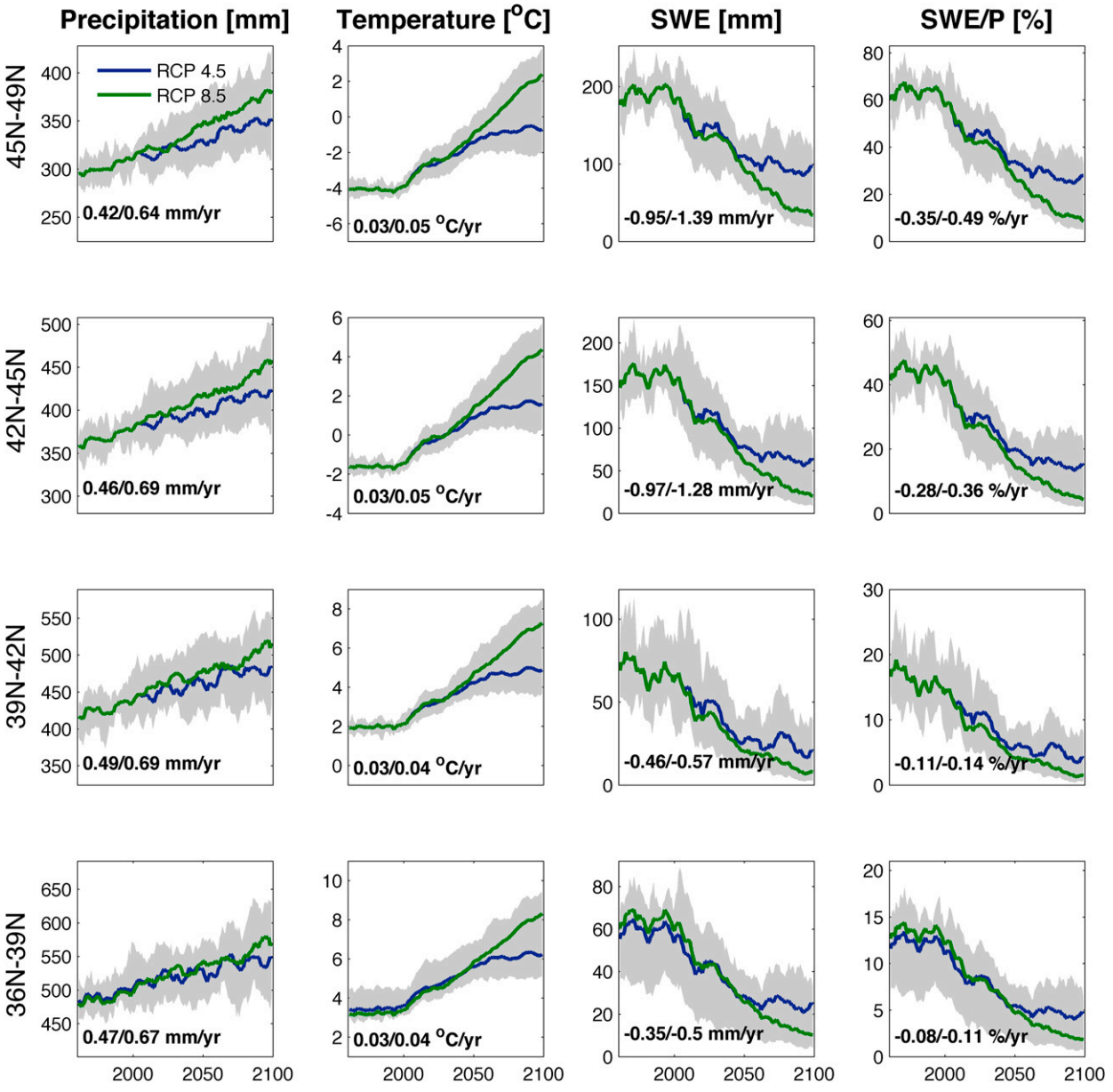

FIG. 2. Temporal changes, from left to right, in seasonal (November–April) total precipitation, mean temperature, VIC-simulated snow water equivalent (SWE), and the ratio between SWE and precipitation. Each panel shows the magnitude of the linear trends for the RCP 4.5 and 8.5 trajectories for the model ensemble mean. The gray envelope represents the 5th–95th percentile of the 10 climate models. Seasonal values are smoothed with an 11-yr running mean.

elevations, is the interpolation processes undergone by observed precipitation fields used to drive the hydrological model (Mote et al. 2005).

b. *Changes in future climatology*

Winter season precipitation and mean temperature projections, for both concentration paths, show a steady increasing trend throughout the twenty-first century by all 10 downscaled GCMs (Fig. 2). The uncertainty envelope for the climate projections was obtained by computing for each season and for each GCM the 5th and 95th percentiles of the different hydrometeorological variables. According to the RCP 4.5 and 8.5 concentration paths, the area-average increase per year in seasonal precipitation is $0.46\,\mathrm{mm\,yr^{-1}}$ (ranging from 0.42 to $0.49\,\mathrm{mm\,yr^{-1}}$) and $0.67\,\mathrm{mm\,yr^{-1}}$ (0.64 to $0.69\,\mathrm{mm\,yr^{-1}}$), respectively. Mean temperatures are also projected to increase $0.03^{\circ}\mathrm{C\,yr^{-1}}$ under the RCP 4.5

TABLE 2. Changes in the magnitude of precipitation (Prec.), temperature (Temp.), and SWE at the end of the twenty-first century. Percentage changes are with respect to the year 1951.

		36°–39°N	39°–42°N	42°–45°N	45°–49°N
RCP 4.5	Prec. (%)	14.6	17.6	19.0	21.2
	Temp. (°C)	3.9	4.1	4.6	4.8
	SWE (%)	−75.9	−84.3	−77.0	−65.2
RCP 8.5	Prec. (%)	21.2	25.0	29.3	33.7
	Temp. (°C)	6.1	6.4	7.2	7.7
	SWE (%)	−93.4	−100.0	−95.2	−87.6

scenarios and 0.45°C yr^{-1} (ranging from 0.03° to 0.05°C yr^{-1}) under the RCP 8.5 scenario. Despite statistically robust increases in precipitation, SWE, and SWE/P trends toward smaller values by the end of the century suggest a change in the phase of precipitation, an increase in sublimation (not included in the analysis despite being one of VIC simulated variables), an increase of snowpack melt, and/or a decrease in the number of snow events. Trends in SWE range from −0.35 to −0.95 mm yr^{-1} and from −0.5 to −1.39 mm yr^{-1} under the RCP 4.5 and 8.5 concentration paths, respectively. The magnitude of the decrease in SWE increases with latitude under both concentration paths in response to warming increases. The projections diverge by the mid-twenty-first century in terms of the magnitude of the projected warming, whereas differences in projected precipitation trends seem to occur earlier in the century. Trends in the GCM ensemble mean were found to be statistically significant at a 95% confidence level for all four variables.

Table 2 shows changes in precipitation, temperature, and SWE between the years 1951 and 2099. Positive changes in both precipitation and temperature are projected by climate models with larger changes at higher latitudinal bands. Under the RCP 4.5 trajectory, precipitation increases between 14% and 21% by the year 2099, whereas temperature increases between 3.9° and 4.8°C. Wetter and warmer conditions are projected under the RCP 8.5 path with changes in precipitation ranging from 21% to 33% and in temperature from 6.1° to 7.7°C. The northernmost latitudinal band experiences the smallest reductions in SWE, ranging from 65% to 87% for the RCP 4.5 and 8.5 trajectories, respectively, whereas reductions in the three southern latitudinal bands ranges from 77% to 84% for the RCP 4.5 and from 93% to 100% for the RCP 8.5 trajectory, suggesting that by the end of the century these regions will likely be snow-free.

One of the expected impacts of warmer temperatures is the reduction in the volume and the duration of the snowpack with decreases in the SWE explained by changes in precipitation phase (from solid to liquid) (Huntington et al. 2004; Knowles et al. 2006). To identify the possible causes of a decline in the SWE, the total number of wet and snow days per year was computed with Eq. (1). For each climate model, changes in the number of snow days between the historical and the future periods were calculated. Table 3a shows that under warmer future climates, the number of snow days is projected to be reduced between 13.6% (45.7%) in the RCP 4.5 trajectory for northern (southern), and by 25% (59%) for northern (southern) latitudinal area under the RCP 8.5 path. Mean changes in the number of snow days were found to be statistically different from zero as supported by the Wilcoxon test at a 95% confidence level. Conversely, the number of precipitation days (liquid and snow) will likely increase (Table 3b) by the second half of the century between 9% (13%) and 14% (22%) for the RCP 4.5 (8.5) trajectories, respectively. The rate of larger decreases in snow days compared to the increase of days with precipitation (solid and liquid) suggest that rainfall events will dominate winter–spring precipitation in the NE-UM region.

c. *Changes in snow depth seasonality and with elevation*

Since changes in snow cover onset and end dates can have important implications for vegetation and wildlife (Grippa et al. 2005; Humphries et al. 2004), this section analyzes the future changes in snow depth throughout the winter season in the four latitudinal bands (Fig. 3) and with elevation (Figs. 4 and 5). The largest proportional decreases in snow depth occur at the beginning (November) and the end (March and April) of the snow season when the snow depth is lower. The snowpack will likely be reduced by more than 50% in the second half of this century in all latitudinal bands in the months of November, December, February, and March under the RCP 4.5 concentration trajectory, with the exception of the northernmost band (45°–49°N) that will experience smaller decreases (Fig. 3a). During the month of April, all the latitudinal bands are projected to lose an average 80% of the snow cover. Under the RCP 8.5 concentration trajectory (Fig. 3b), all four latitudinal bands will likely experience decreases in snow coverage of 50% or more throughout the winter season, with the largest decreases found in the shoulder snow season (November, March, and April). These results indicate that the length of the snow season will likely be reduced in the second half of the twenty-first century, and that the majority of the losses in the snowpack will occur at the beginning of the spring season, which might have direct impacts on spring streamflow peaks.

The NE-UM region is predominately situated at low topographic elevations (Fig. 1b). For instance, in the VIC model setup, approximately 70% of the grid cells

TABLE 3. Percentage change (%) in the number of VIC-simulated days with (a) solid and (b) liquid precipitation between the future period (2041–95) and the historical period (1951–2005) for the 10 statistically downscaled climate models. Changes are average for each latitudinal band. The snow season encompasses the months of November through April. Bold numbers indicate changes in the mean that are statistically significant at the 95% confidence level.

	(a) Changes in number of days with solid precipitation							
	RCP 4.5				RCP 8.5			
Model/band	36°–39°N	39°–42°N	42°–45°N	45°–49°N	36°–39°N	39°–42°N	42°–45°N	45°–49°N
BCC-CSM1.1	**−48.3**	**−42.0**	**−28.6**	**−19.9**	**−60.8**	**−52.5**	**−40.5**	**−27.3**
CCSM4	**−54.6**	**−42.0**	**−28.6**	**−11.8**	**−57.8**	**−47.9**	**−37.9**	**−23.8**
CESM1-BGC	**−38.5**	**−32.0**	**−22.4**	**−16.4**	**−57.0**	**−46.0**	**−33.4**	**−22.8**
CNRM-CM5	**−52.1**	**−40.8**	**−24.8**	**−13.0**	**−61.3**	**−54.4**	**−39.1**	**−25.2**
CSIRO-Mk3.6.0	**−53.9**	**−42.1**	**−25.6**	**−8.3**	**−64.7**	**−53.6**	**−37.0**	**−17.3**
FIO-ESM	**−23.3**	**−21.4**	**−18.5**	**−12.4**	**−46.2**	**−45.1**	**−38.2**	**−27.8**
GFDL-ESM2G	−33.4	**−25.6**	**−12.6**	**−3.8**	**−49.8**	**−38.4**	**−26.4**	**−10.8**
IPSL-CM5A-MR	**−55.8**	**−45.4**	**−30.8**	**−22.1**	**−71.3**	**−62.8**	**−49.4**	**−40.6**
MIROC5	**−56.3**	**−47.6**	**−32.8**	**−15.2**	**−71.0**	**−62.5**	**−51.8**	**−32.3**
NorESM1-M	**−43.3**	**−34.6**	**−25.6**	**−12.5**	**−60.3**	**−49.4**	**−38.3**	**−22.5**
Ensemble mean	**−45.7**	**−37.2**	**−25.0**	**−13.6**	**−59.8**	**−51.2**	**−39.2**	**−25.1**
	(b) Changes in number of days with precipitation (solid and liquid)							
	RCP 4.5				RCP 8.5			
Model/band	36°–39°N	39°–42°N	42°–45°N	45°–49°N	36°–39°N	39°–42°N	42°–45°N	45°–49°N
BCC-CSM1.1	**6.1**	**7.7**	9.7	14.3	**14.7**	**17.7**	**22.1**	**28.3**
CCSM4	**13.9**	**9.0**	**8.4**	**14.0**	**22.9**	**18.3**	**16.8**	**21.0**
CESM1-BGC	**13.8**	**17.6**	**15.2**	**10.8**	**19.3**	**24.0**	**22.9**	**22.5**
CNRM-CM5	**10.3**	**13.8**	**14.1**	**15.0**	**12.7**	**16.2**	**18.0**	**20.4**
CSIRO-Mk3.6.0	**10.8**	**16.2**	**17.0**	**16.0**	3.0	**12.1**	**19.8**	**25.0**
FIO-ESM	**12.8**	**10.5**	5.0	4.2	**14.1**	**11.8**	**9.4**	8.2
GFDL-ESM2G	**7.6**	**10.1**	**14.2**	18.5	**15.5**	**18.6**	**23.3**	**29.5**
IPSL-CM5A-MR	0.9	5.2	7.5	**9.0**	−5.0	1.5	6.5	**8.9**
MIROC5	**9.7**	**14.9**	**16.6**	**20.3**	**15.4**	**19.2**	**19.7**	**27.8**
NorESM1-M	3.2	**9.0**	**13.6**	**17.7**	**13.0**	**19.5**	**24.6**	**30.1**
Ensemble mean	**8.9**	**11.4**	**12.1**	**14.0**	**12.6**	**15.9**	**18.3**	**22.2**

have average elevations below 400 m (1312 ft), 16% of the grid cells are located between 400- and 600-m elevation, and the rest are above 600 m. Decreases in the snowpack will be larger in low elevations throughout the entire season. Under the RCP 4.5 trajectory, negative changes greater than 50% will be found at elevations below 200 m (Fig. 3c), whereas under the RCP 8.5 path 50% reductions will be found at all elevation bands (Fig. 3d). The loss of snowpack will be more significant in early spring (March and April) for the RCP 4.5 path, but more equally distributed throughout the season in the RCP 8.5 path.

The long-term changes over the entire 149-yr simulation period reveal statistically significant negative trends in snow depth within both elevation and latitudinal bands (Fig. 4). All trends of the ensemble mean are tested for significance using the Mann–Kendall test. Despite total seasonal values being smoothed with an 11-yr moving average window, snow depths show significant interannual variability superimposed upon the negative changes over time. The magnitude of the Sen's slope is larger at higher latitudinal bands (42°–45°N and 45°–49°N), with trends ranging from −0.27 to $-1.03\,\mathrm{cm\,yr^{-1}}$. Within these latitudinal bands, negative trends at elevations higher than 600 m are the largest in the region. At lower elevations (i.e., less than 400 m) and in the southernmost latitudinal bands, the snowpack is likely to disappear by the end of the century with trends ranging from $-0.1\,\mathrm{cm\,yr^{-1}}$ (ranging from -0.04 to $-0.17\,\mathrm{cm\,yr^{-1}}$) under the RCP 4.5 path to $-0.17\,\mathrm{cm\,yr^{-1}}$ (-0.05 to $-0.21\,\mathrm{cm\,yr^{-1}}$) under the RCP 8.5 path.

The slope spatial variability with elevation and latitude can be best visualized in Fig. 5. Statistically significant trends are found in 69% of the study domain with the largest increases in precipitation seen in high elevations and at higher latitudes under both concentration paths (Figs. 5a,b) (note that elevations above 775 m and latitudes larger than 45.5° are not included in the plot due to the limited number of grid cells in those latitudinal and altitudinal bands). The strongest decreases in SWE locate at higher latitudes and elevations,

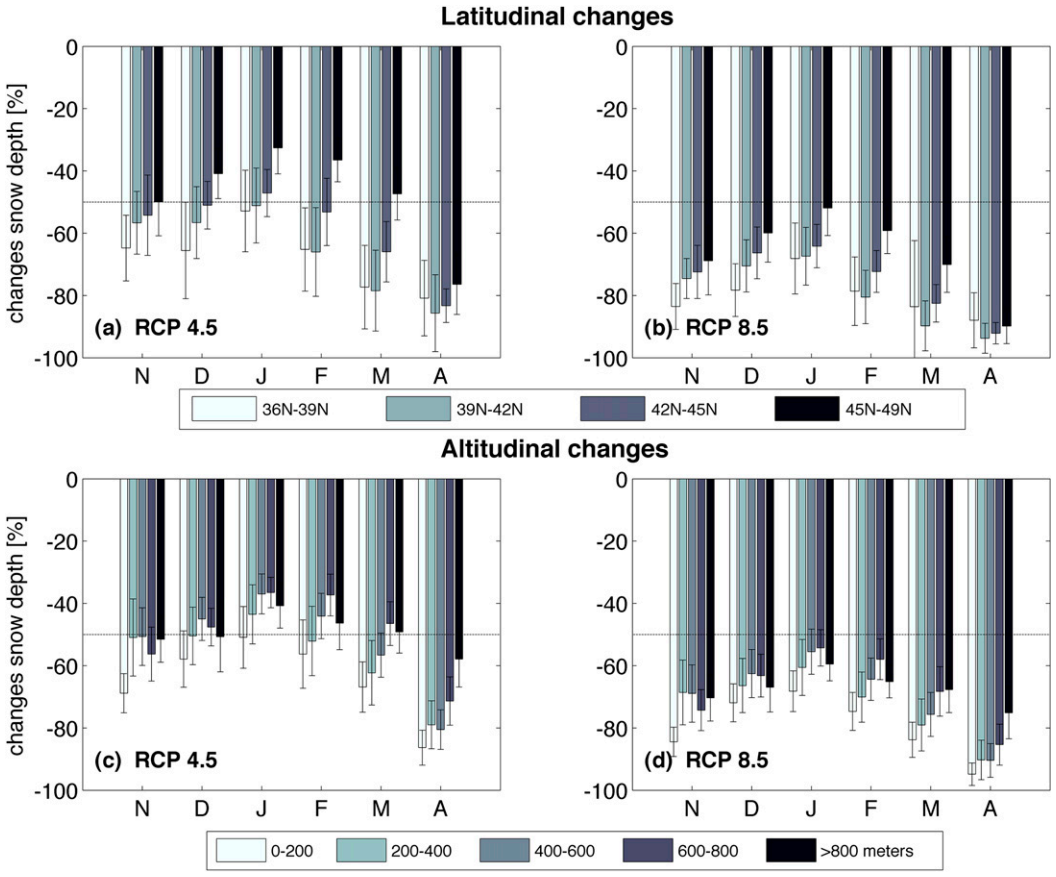

FIG. 3. Latitudinal and altitudinal changes in the seasonal cycle of ensemble mean snow depth between the historical (1951–2005) and future (2041–95) periods. Values are expressed as percentage changes from the historical period. The error bars show the intermodel standard deviation and the horizontal dotted line shows 50% changes.

indicating that, as a result, the fastest declines in projected snow occur at higher elevations in the Appalachian Mountains. The trends in SWE are statistically significant for the highest elevations (above 600 m) and for latitudes north of 42°N, while those for lower elevations and southern latitudes are not statistically robust.

To estimate the probability that the NE-UM will be snow covered in the future, we compute the spatial distribution of the marginal probability of snow cover exceeding a determined threshold in the historical record, and how this probability changes by the second half of the twenty-first century. Figure 6 shows the probability of occurrence of monthly mean snow depth equal or larger than 2.5, 5.0, 10, and 20 cm (approximately 1 to 8 in.) for the month of February, when the snowpack reaches its maximum in the observed record. Plots in Figs. 6a–d show that during the historical period, most of the region has a 80% probability of being covered, on average, by up to 5.0 cm of snow in the month of February in latitudes higher than 40°N, and the probability decreases southward. For snow depths of 10 cm, high probabilities of occurrence are restricted to the northeastern corner of the domain (New England) and to Great Lakes regions, whereas southern areas have fading north-to-south probabilities ranging from 50% to 0%. For future climate projections (Figs. 6e–l), the area covered by 20-cm snow depths will hardly exist under both concentration paths except for New England. Present-day snow depth conditions will be reduced by 50% in the RCP 4.5 and by 75% in the RCP 8.5 trajectory, as climate gets warmer. Note that VIC simulations tend to underestimate snow cover in the northwest corner of the domain (see Fig. 1d); therefore the decrease in snow cover in that area might be larger. Results indicate that in the period 2041–95, a snow depth of 10 cm will have the same probability of occurrence that a 20-cm depth had during the historical record (Figs. 6d,g). Similarly under the RCP 8.5 trajectory, a 5-cm snow depth will have a comparable probability of occurrence as the probability of the historical 20-cm snow depth.

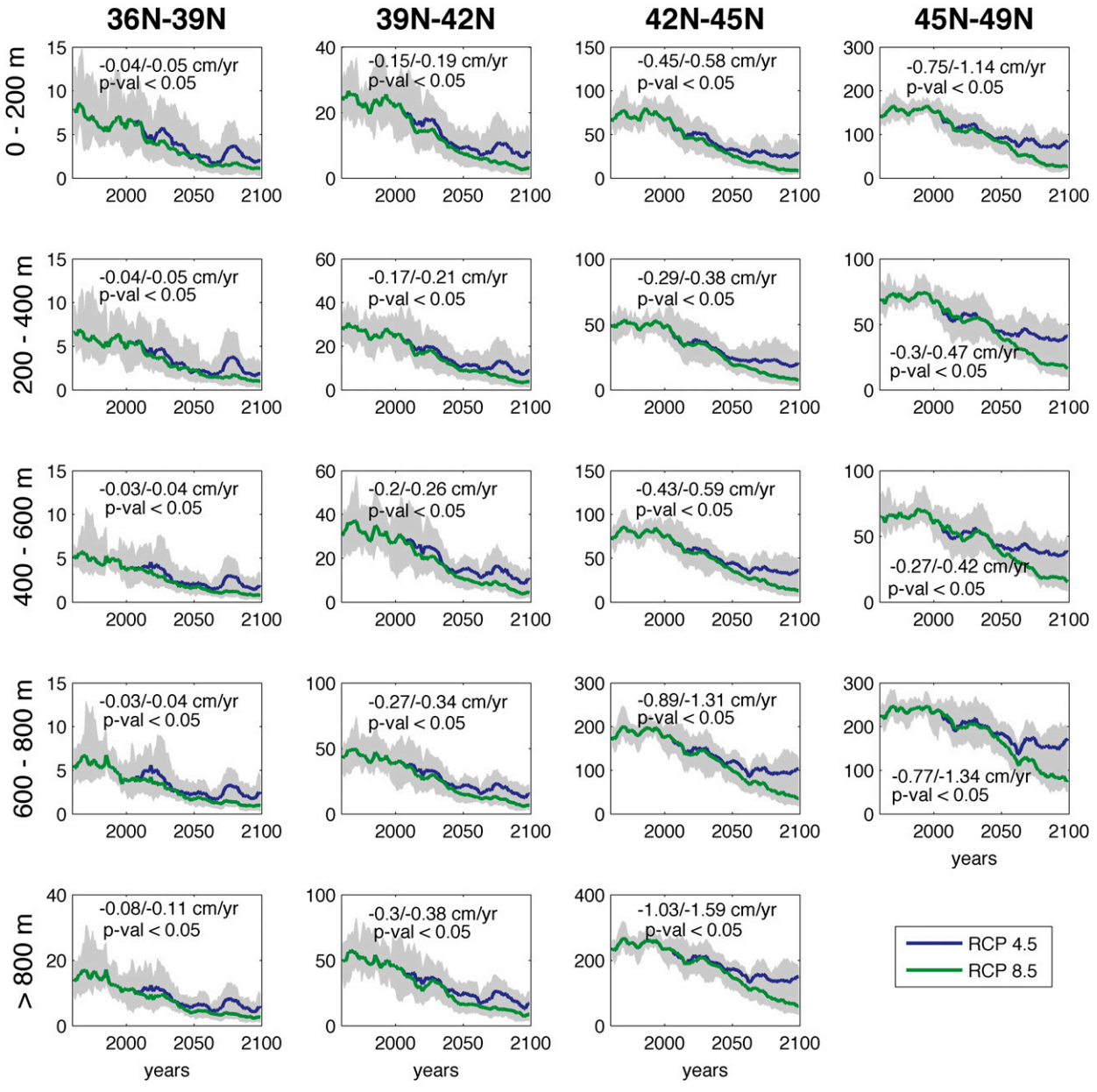

FIG. 4. Temporal changes in mean seasonal snow depth along latitudinal bands (~3° spacing) and elevation bands (200-m intervals). The magnitude of the linear trend (cm yr^{-1}) and its statistical significance are indicated inside of each plot for the RCP 4.5 and 8.5 concentration paths. The gray envelope shows the 5th to 95th percentile, and the solid lines show the climate model ensemble mean.

d. Spring (MAM) streamflow characteristics linked to snowmelt

To evaluate how changes in spring snow coverage can affect maximum peak runoffs, we simulated streamflows in 124 basins using precipitation and temperature forcings from the 10 selected GCMs. Daily streamflow simulations were first smoothed with a 3-day moving average window to minimize the effect of outliers in the analysis. For each year and each GCM, the basin's maximum spring streamflow and the day of its occurrence were selected. A multimodel ensemble mean was computed for the 10 GCMs. To enable comparison between basins, the magnitude of the flows were normalized by the respective size of the basin. Figure 7 shows changes in the timing and magnitude of the maximum spring peak flow between the future and the historical periods. The numbers between brackets indicate the number of basins with positive or negative changes as a percentage of the total number of basins.

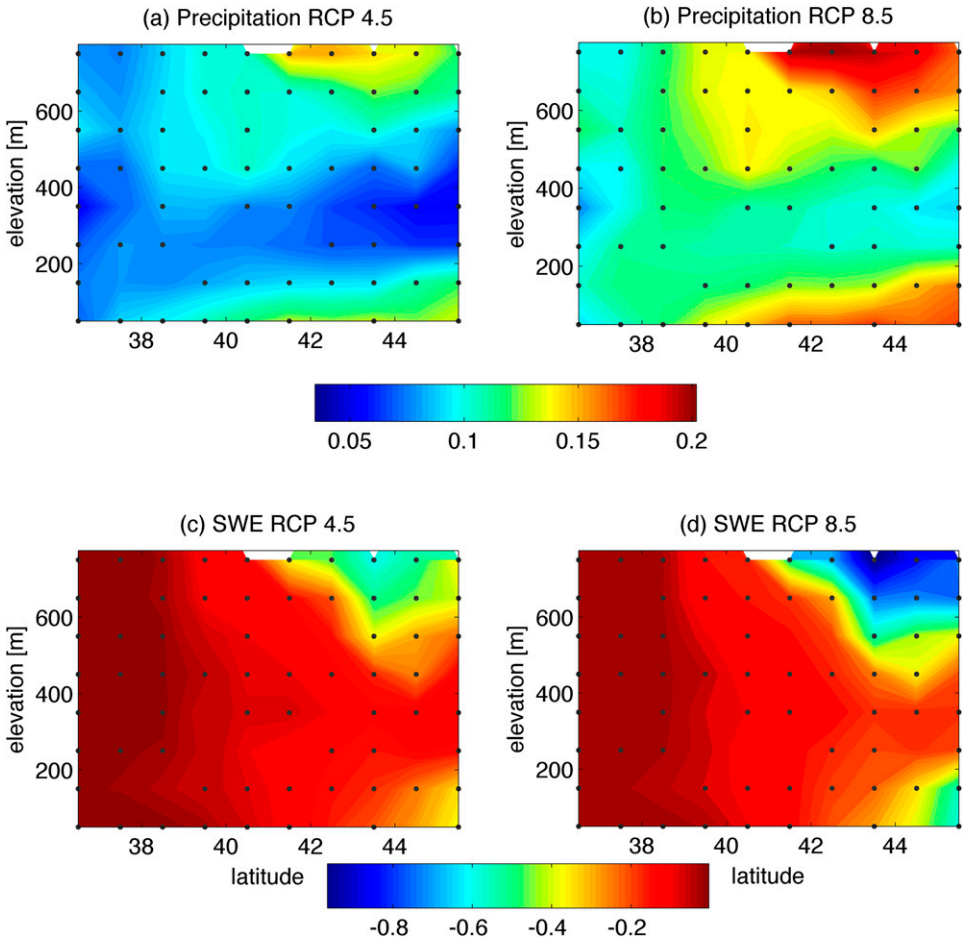

FIG. 5. Slope of the linear trend of winter (November–April) (a),(b) precipitation and (c),(d) SWE in mm yr^{-1} for RCP (left) 4.5 and (right) 8.5. Dots represent statistically significant trends.

A positive change indicates the peak occurs later in the season whereas a negative change indicates an earlier occurrence. The nonparametric Wilcoxon test on medians was used to assess the statistical significance of the changes (p values less than 0.05 are considered to be statistically significant). Under the RCP 4.5 trajectory, the ensemble mean shows that the timing of the spring peak flows is likely to occur earlier in the season in 83% of the basins. Spring flow peaks are projected to occur for most basins 1 to 15 days earlier than the historical spring peak flows; however, a majority of the basins show early peaks on the order of 5 days. The earlier timing becomes less marked for RCP 8.5 simulations, with 42% of the basins showing negative (earlier) times, perhaps as result of the reduced snowpack. Notably, earlier peaks are consistently being projected for the future in the northeast corner of the region (states of Maine, New Hampshire, Vermont, Massachusetts, and New York) and in the Great Lakes region. The magnitude of peak flows (Figs. 7c,d) will increase in almost ⅔ of the basins under both concentration paths, with most of these increases located at lower latitudes. In the future, peak flows will range from 5% to 25% higher than the historical period. Negative changes (decreases) seem to be restricted to latitudes north of 40°N, and in particular to the New England states and New York, where peaks are projected to decrease by as much as 35% in some basins.

In snow-dominated environments, a widely used statistical measure to evaluate changes in catchment dynamic due to changes in snowmelt is the center timing (CT). Low CT values imply that the basin is yielding more water due to an earlier-than-normal melting of the snowpack if precipitation amounts do not decrease. For each latitudinal band, we computed the CT for each water year, defined as 1 August to 31 July, and averaged them for the basins in the band. Trends in CT, and changes between the future (2041–95) and the historical period, are shown in Table 4. In the future, the occurrence of the CT shifts to earlier in

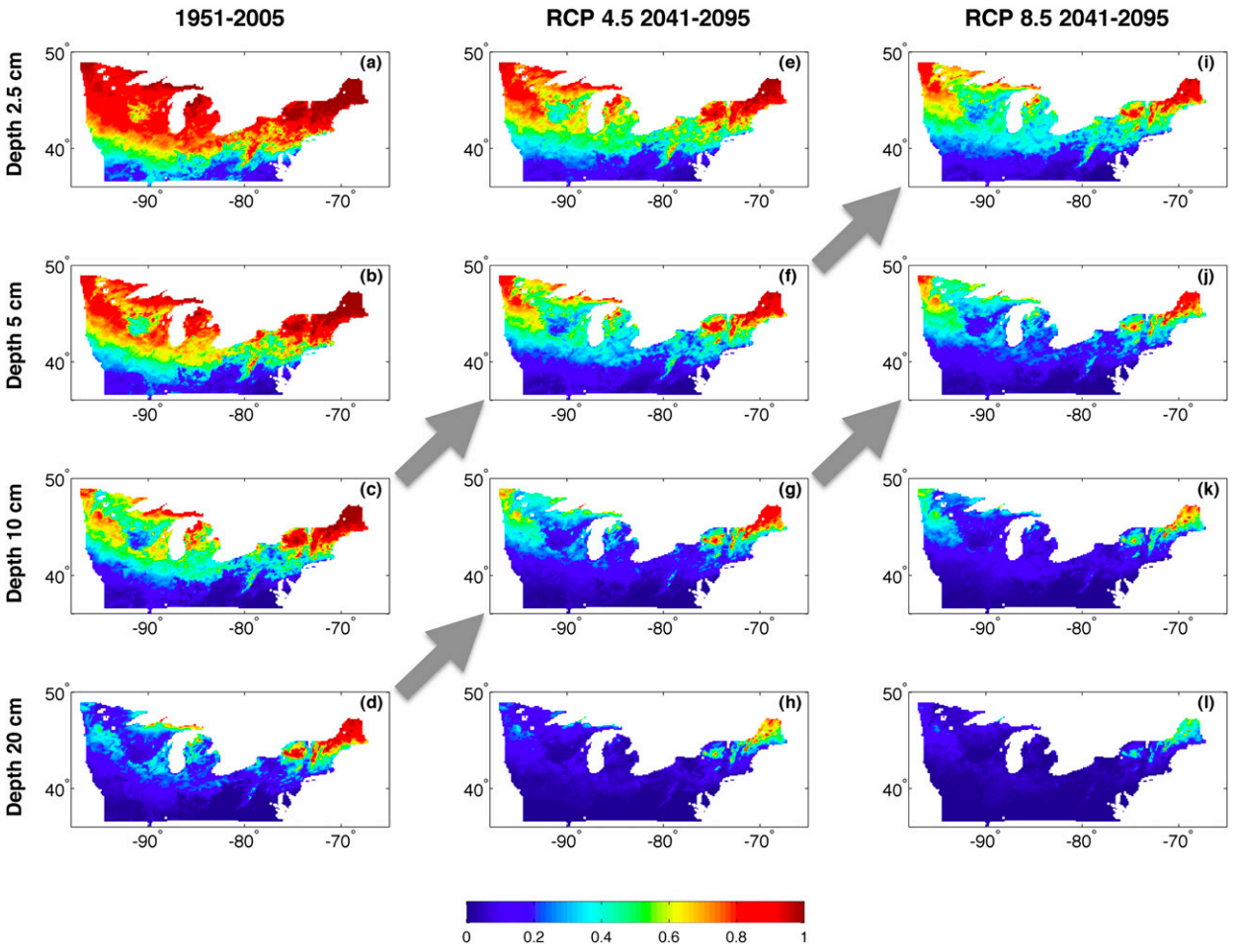

FIG. 6. Marginal probability of February ensemble mean snow depth exceeding a certain threshold, for the (left) historical period, and the future period (middle) RCP 4.5 and (right) RCP 8.5 trajectories.

the year in the two northernmost latitudinal bands (42°–45°N and 45°–49°N), with statistically robust negative trends ranging from −0.16 to −0.09 days yr^{-1} in the RCP 4.5 concentration path and from −0.2 and −0.09 days yr^{-1} in the RCP 8.5 concentration path for each band, respectively. For all the basins, CTs are projected to occur on average 22 to 27 days earlier in the 42°–45°N by the end of the twenty-first century. In the 45°–49°N latitude band, climate simulated CTs occur 13 days earlier, whereas in the 39°–42°N bands the changes range between 6–8 days earlier for RCP 4.5 and 8.5, respectively. Earlier CTs in the northern bands are likely linked to the stronger negative trends in SWE shown in Fig. 4 compared to the southern bands. We speculate that the proximity of the basins to the Atlantic coast might be an important factor influencing the changes. Future analysis need to include longitudinal bands to evaluate differences between maritime versus continental climate conditions.

4. Conclusions

The depth of the snowpack and the length of the snow season are of fundamental importance for natural ecosystems in the Northeast and upper Midwest United States. Our study uses statistically downscaled CMIP5 future climate projections from 10 climate models and a hydrological model to evaluate future changes in snow cover during the snow season (November–April) in the region. It also assesses changes in the magnitude and timing of spring maximum streamflows in 124 selected basins. Climate simulations under two representative concentration paths: RCP 4.5 and RCP 8.5 are included in the analysis.

Precipitation and mean temperature are projected to increase in the twenty-first century during the snow season, with statistically significant trends being larger at higher latitudes. However, despite sustained increases in precipitation, the SWE multimodel ensemble mean

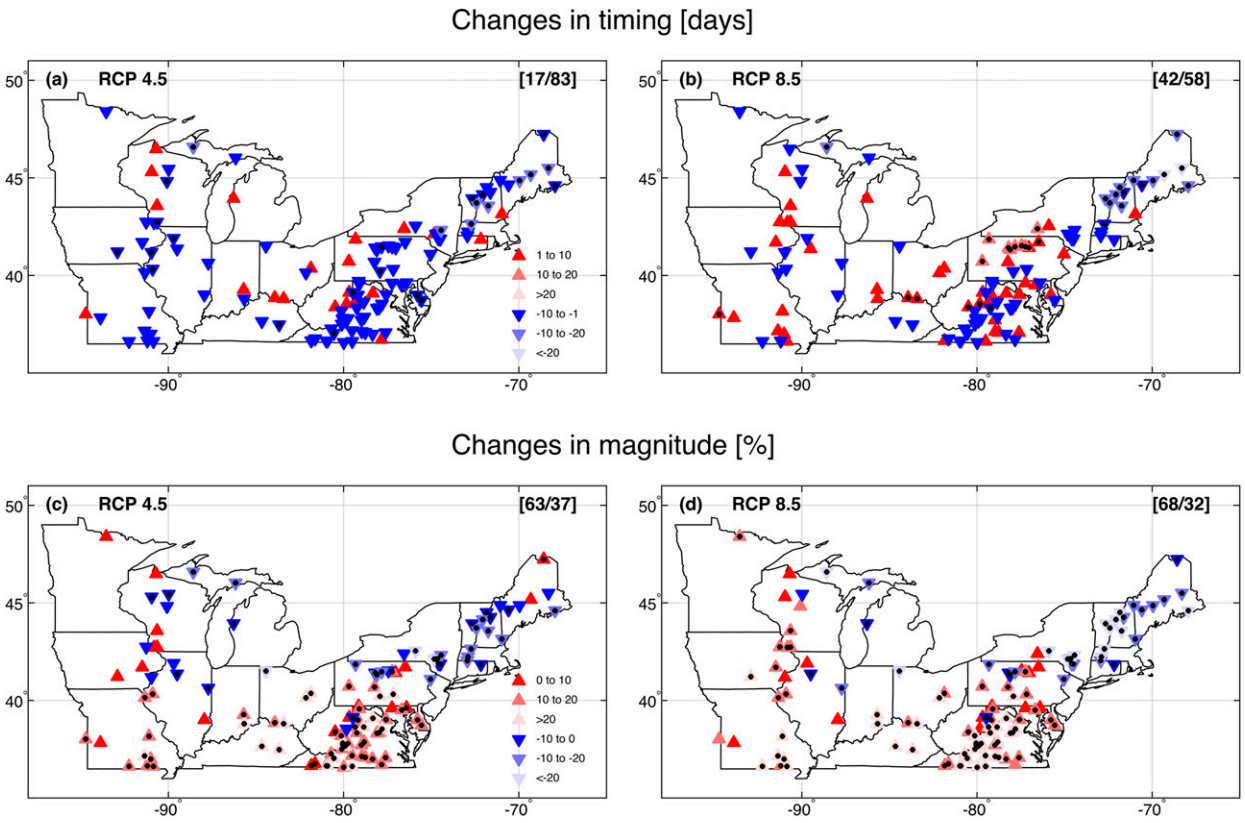

FIG. 7. Changes in the (a),(b) timing and (c),(d) magnitude of maximum spring streamflow between (left) the future period (2041–95) and (right) the historical period (1951–2005). Positive (negative) changes are indicated with red (blue) upward (downward) pointing triangles; the numbers between brackets represent the number of positive (negative) cases. The stippling indicates changes in the median statistically significant at 95% confidence level.

projection shows a strong decreasing trend throughout the century for the region, suggesting that the southern latitudinal bands (south of 42°N) will be almost snow-free by the end of the century. The rate of decline in snowpack is expected to be larger at higher elevations and northern latitudes. Snowpack of 20 cm or more are projected to hardly exist in the month of February by the second half of the century. The probability of occurrence of present-day snowpack conditions will be reduced by more than half in the second half of the century, indicating that snow cover will migrate northward over time. The seasonality of snow cover will likely change in second half of the twenty-first century, with the larger decreases during early spring (March and April) under the RCP 4.5 concentration path. Decreases will be more uniformly distributed throughout the season under the RCP 8.5 trajectory.

By the second half of the century, spring (MAM) peak flows are projected to occur earlier in the season in more than 80% of the basins throughout the region under the RCP 4.5 trajectory. Earlier peak arrivals are less marked under the RCP 8.5 trajectory, perhaps as result of a decreasing snow cover. The magnitude of the spring peak flows will likely increase in $^2/_3$ of the basins, with most of the increases occurring in basins located at lower latitudes. Conversely, decreases in peak magnitudes are restricted to basins located in the northern regions (north of 40°N), and in particular to New England and New York state, where decreases will reach up to 35% with respect to the historical period.

TABLE 4. Slope of linear trend in the period 1951–2099 and changes in center timing (CT) between the historical (1951–2005) and future (2041–95) periods. The CT is computed for each year and basin, and consequently averaged for each latitudinal band.

	Slope of linear trend period 1951–2099 (days yr^{-1})		Changes in center timing ensemble mean (days)	
Latitude band	RCP 4.5	RCP 8.5	RCP 4.5	RCP 8.5
36°–39°N	−0.01	−0.03	1.0	4.0
39°–42°N	−0.05	−0.06	6.0	8.0
42°–45°N	−0.16	−0.2	22.0	27.0
45°–49°N	−0.09	−0.09	13.0	13.0

The center timing will likely occur, on average, 22 to 27 days earlier in the northern basins (latitudes 42°–45°N) by the end of the century, which indicates changes in basin dynamics due to changes in snowmelt, whereas southern basins (latitudinal bands 39°–42°N) will experience smaller changes. This physical mechanism has been documented for basins in the western United States (Hidalgo et al. 2009; Stewart et al. 2005).

Declines in future snow coverage in the region indicate that increases in precipitation cannot offset increases in temperature, which will affect ecosystem functioning and compromise their long-term sustainability. This conclusion should also be weighed with an understanding of the modeling process. First, VIC simulations driven with observations tend to underestimate observed snow in the Great Lakes region, and therefore changes are likely to be underestimated in the future. Second, VIC simulations assume a static representation of vegetation coverage, so the future interaction between snow and vegetation might not be realistically represented. Third, snow fields are not simulated directly for the GCM models but rather indirectly estimated with the VIC model, hence simulations implicitly use the coarse topography of the hosting GCM. As a result, the true decreases in snow coverage with elevation are likely to be larger than the ones found in this study.

Acknowledgments. Funding was provided by the Department of Interior Northeast Climate Science Center (Grant 111-1485). The authors are grateful to WCRP for its role in making available the CMIP5 dataset. We thank Dr. Keith Nislow for his valuable comments, and Dr. Austin Polebitski and Dr. Scott Steinschneider for their help obtaining the Gauges II dataset. We are grateful to two anonymous reviewers whose careful review and helpful comments led to substantial improvements to this work.

REFERENCES

Andreadis, K. M., P. Storck, and D. P. Lettenmaier, 2009: Modeling snow accumulation and ablation processes in forested environments. *Water Resour. Res.*, **45**, W05429, doi:10.1029/2008WR007042.

Barnett, T. P., J. C. Adam, and D. P. Lettenmaier, 2005: Potential impacts of a warming climate on water availability in snow-dominated regions. *Nature*, **438**, 303–309, doi:10.1038/nature04141.

Brown, R. D., 2000: Northern Hemisphere snow cover variability and change, 1915–97. *J. Climate*, **13**, 2339–2355, doi:10.1175/1520-0442(2000)013<2339:NHSCVA>2.0.CO;2.

——, and D. A. Robinson, 2011: Northern Hemisphere spring snow cover variability and change over 1922–2010 including an assessment of uncertainty. *Cryosphere*, **5**, 219–229, doi:10.5194/tc-5-219-2011.

——, B. Brasnet, and D. A. Robinson, 2003: Gridded North American monthly snow depth and snow water equivalent for GCM evaluation. *Atmos.–Ocean*, **41**, 1–14, doi:10.3137/ao.410101.

Choi, G., D. A. Robinson, and S. Kang, 2010: Changing Northern Hemisphere snow seasons. *J. Climate*, **23**, 5305–5310, doi:10.1175/2010JCLI3644.1.

Comte, L., L. Buisson, M. Daufresne, and G. Grenouillet, 2013: Climate-induced changes in the distribution of freshwater fish: Observed and predicted trends. *Freshwater Biol.*, **58**, 625–639, doi:10.1111/fwb.12081.

Cotton, P. A., 2003: Avian migration phenology and global climate change. *Proc. Natl. Acad. Sci. USA*, **100**, 12 219–12 222, doi:10.1073/pnas.1930548100.

Crick, H. Q. P., 2004: The impact of climate change on birds. *Ibis*, **146**, 48–56, doi:10.1111/j.1474-919X.2004.00327.x.

Das, T., and Coauthors, 2009: Structure and detectability of trends in hydrological measures over the western United States. *J. Hydrometeor.*, **10**, 871–892, doi:10.1175/2009JHM1095.1.

——, M. D. Dettinger, D. R. Cayan, and H. G. Hidalgo, 2011: Potential increase in floods in California's Sierra Nevada under future climate projections. *Climatic Change*, **109**, 71–94, doi:10.1007/s10584-011-0298-z.

Demaria, E. M. C., E. P. Maurer, B. Thrasher, S. Vicuña, and F. J. Meza, 2013: Climate change impacts on an alpine watershed in Chile: Do new model projections change the story? *J. Hydrol.*, **502**, 128–138, doi:10.1016/j.jhydrol.2013.08.027.

——, R. N. Palmer, and J. K. Roundy, 2016: Regional climate change projections of streamflow characteristics in the Northeast and Midwest U.S. *J. Hydrol. Reg. Stud.*, **5**, 309–323, doi:10.1016/j.ejrh.2015.11.007.

Derksen, C., and R. Brown, 2012: Spring snow cover extent reductions in the 2008–2012 period exceeding climate model projections. *Geophys. Res. Lett.*, **39**, L19504, doi:10.1029/2012GL053387.

Dominguez, F., J. Cañon, and J. Valdes, 2010: IPCC-AR4 climate simulations for the Southwestern US: The importance of future ENSO projections. *Climatic Change*, **99**, 499–514, doi:10.1007/s10584-009-9672-5.

Duan, Q. Y., S. Sorooshian, and V. Gupta, 1992: Effective and efficient global optimization for conceptual rainfall-runoff models. *Water Resour. Res.*, **28**, 1015–1031, doi:10.1029/91WR02985.

Dyer, J. L., and T. L. Mote, 2006: Spatial variability and trends in observed snow depth over North America. *Geophys. Res. Lett.*, **33**, L16503, doi:10.1029/2006GL027258.

Falcone, J. D., D. M. Carlisle, D. M. Wolock, and M. R. Meador, 2010: GAGES: A stream gage database for evaluating natural and altered flow conditions in the conterminous United States. *Ecology*, **91**, 621, doi:10.1890/09-0889.1.

Grabowski, M. M., F. I. Doyle, D. G. Reid, D. Mossop, and D. Talarico, 2013: Do Arctic-nesting birds respond to earlier snowmelt? A multi-species study in north Yukon, Canada. *Polar Biol.*, **36**, 1097–1105, doi:10.1007/s00300-013-1332-6.

Grippa, M., L. Kergoat, T. Le Toan, N. M. Mognard, N. Delbart, J. L'Hermitte, and S. M. Vicente-Serrano, 2005: The impact of snow depth and snowmelt on the vegetation variability over central Siberia. *Geophys. Res. Lett.*, **32**, L21412, doi:10.1029/2005GL024286.

Gutmann, E., T. Pruitt, M. P. Clark, L. Brekke, J. R. Arnold, D. A. Raff, and R. M. Rasmussen, 2014: An intercomparison of statistical downscaling methods used for water resource assessments in the United States. *Water Resour. Res.*, **50**, 7167–7186, doi:10.1002/2014WR015559.

Hayhoe, K., and Coauthors, 2007: Past and future changes in climate and hydrological indicators in the US Northeast. *Climate Dyn.*, **28**, 381–407, doi:10.1007/s00382-006-0187-8.

Hidalgo, H. G., and Coauthors, 2009: Detection and attribution of streamflow timing changes to climate change in the western United States. *J. Climate*, **22**, 3838–3855, doi:10.1175/2009JCLI2470.1.

Humphries, M. M., J. Umbanhowar, and K. S. McCann, 2004: Bioenergetic prediction of climate change impacts on northern mammals. *Integr. Comp. Biol.*, **44**, 152–162, doi:10.1093/icb/44.2.152.

Huntington, T. G., G. A. Hodgkins, B. D. Keim, and R. W. Dudley, 2004: Changes in the proportion of precipitation occurring as snow in New England (1949–2000). *J. Climate*, **17**, 2626–2636, doi:10.1175/1520-0442(2004)017<2626:CITPOP>2.0.CO;2.

Kapnick, S. B., and T. L. Delworth, 2013: Controls of global snow under a changed climate. *J. Climate*, **26**, 5537–5562, doi:10.1175/JCLI-D-12-00528.1.

Kendall, M. G., 1975: *Rank Correlation Methods.* 5th ed. Oxford University Press, 272 pp.

Knowles, N., M. D. Dettinger, and D. R. Cayan, 2006: Trends in snowfall versus rainfall in the western United States. *J. Climate*, **19**, 4545–4559, doi:10.1175/JCLI3850.1.

Knutti, R., and J. Sedlacek, 2013: Robustness and uncertainties in the new CMIP5 climate model projections. *Nat. Climate Change*, **3**, 369–373, doi:10.1038/nclimate1716.

Krasting, J. P., A. J. Broccoli, K. W. Dixon, and J. R. Lanzante, 2013: Future changes in Northern Hemisphere snowfall. *J. Climate*, **26**, 7813–7828, doi:10.1175/JCLI-D-12-00832.1.

Liang, X., D. P. Lettenmaier, E. F. Wood, and S. J. Burges, 1994: A simple hydrologically based model of land-surface water and energy fluxes for general circulation models. *J. Geophys. Res.*, **99** (D7), 14 415–14 428, doi:10.1029/94JD00483.

——, E. F. Wood, and D. P. Lettenmaier, 1996: Surface soil moisture parameterization of the VIC-2L model: Evaluation and modification. *Global Planet. Change*, **13**, 195–206, doi:10.1016/0921-8181(95)00046-1.

Lohmann, D., E. Raschke, B. Nijssen, and D. P. Lettenmaier, 1998: Regional scale hydrology: I. Formulation of the VIC-2L model coupled to a routing model. *Hydrol. Sci. J.*, **43**, 131–141, doi:10.1080/02626669809492107.

Maloney, E. D., and Coauthors, 2014: North American climate in CMIP5 experiments: Part III: Assessment of twenty-first-century projections. *J. Climate*, **27**, 2230–2270, doi:10.1175/JCLI-D-13-00273.1.

Mann, H. B., 1945: Nonparametric tests against trend. *Econometrica*, **13**, 245–259, doi:10.2307/1907187.

Maurer, E. P., A. W. Wood, J. C. Adam, D. P. Lettenmaier, and B. Nijssen, 2002: A long-term hydrologically based dataset of land surface fluxes and states for the conterminous United States. *J. Climate*, **15**, 3237–3251, doi:10.1175/1520-0442(2002)015<3237:ALTHBD>2.0.CO;2.

——, L. Brekke, T. Pruitt, and P. B. Duffy, 2007: Fine-resolution climate projections enhance regional climate change impact studies. *Eos, Trans. Amer. Geophys. Union*, **88**, 504, doi:10.1029/2007EO470006.

Mills, L. S., and Coauthors, 2013: Camouflage mismatch in seasonal coat color due to decreased snow duration. *Proc. Natl. Acad. Sci. USA*, **110**, 7360–7365, doi:10.1073/pnas.1222724110.

Mote, P. W., A. F. Hamlet, M. P. Clark, and D. P. Lettenmaier, 2005: Declining mountain snowpack in western North America. *Bull. Amer. Meteor. Soc.*, **86**, 39–49, doi:10.1175/BAMS-86-1-39.

Notaro, M., D. Lorenz, C. Hoving, and M. Schummer, 2014: Twenty-first-century projections of snowfall and winter severity across central-eastern North America. *J. Climate*, **27**, 6526–6550, doi:10.1175/JCLI-D-13-00520.1.

Peng, S., S. Piao, P. Ciais, P. Friedlingstein, L. Zhou, and T. Wang, 2013: Change in snow phenology and its potential feedback to temperature in the Northern Hemisphere over the last three decades. *Environ. Res. Lett.*, **8**, 014008, doi:10.1088/1748-9326/8/1/014008.

Pierce, D. W., and D. R. Cayan, 2013: The uneven response of different snow measures to human-induced climate warming. *J. Climate*, **26**, 4148–4167, doi:10.1175/JCLI-D-12-00534.1.

——, and Coauthors, 2008: Attribution of declining western U.S. snowpack to human effects. *J. Climate*, **21**, 6425–6444, doi:10.1175/2008JCLI2405.1.

Rupp, D. E., P. W. Mote, N. L. Bindoff, P. A. Stott, and D. A. Robinson, 2013: Detention and attribution of observed changes in Northern Hemisphere spring snow cover. *J. Climate*, **26**, 6904–6914, doi:10.1175/JCLI-D-12-00563.1.

Sen, P. K., 1968: Estimates of the regression coefficient based on Kendall's tau. *J. Amer. Stat. Assoc.*, **63**, 1379–1389, doi:10.1080/01621459.1968.10480934.

Shi, X., S. J. Dery, P. Ya. Groisman, and D. P. Lettenmaier, 2013: Relationships between recent pan-Arctic snow cover and hydroclimate trends. *J. Climate*, **26**, 2048–2064, doi:10.1175/JCLI-D-12-00044.1.

Stewart, I. T., D. R. Cayan, and M. D. Dettinger, 2005: Changes toward earlier streamflow timing across western North America. *J. Climate*, **18**, 1136–1155, doi:10.1175/JCLI3321.1.

Storck, P., D. P. Lettenmaier, and S. M. Bolton, 2002: Measurement of snow interception and canopy effects on snow accumulation and melt in a mountainous maritime climate, Oregon, United States. *Water Resour. Res.*, **38**, 1223, doi:10.1029/2002WR001281.

Taylor, K. E., R. J. Stouffer, and G. A. Meehl, 2012: An overview of CMIP5 and the experiment design. *Bull. Amer. Meteor. Soc.*, **93**, 485–498, doi:10.1175/BAMS-D-11-00094.1.

Troy, T. J., E. F. Wood, and J. Sheffield, 2008: An efficient calibration method for continental-scale land surface modeling. *Water Resour. Res.*, **44**, W09411, doi:10.1029/2007WR006513.

Wi, S., F. Dominguez, M. Durcik, J. Valdes, H. F. Diaz, and C. L. Castro, 2012: Climate change projection of snowfall in the Colorado River Basin using dynamical downscaling. *Water Resour. Res.*, **48**, W05504, doi:10.1029/2011WR010674.

Wilks, D. S., 2006: *Statistical Methods in the Atmospheric Sciences.* 2nd ed. Academic Press, 627 pp.

Wood, A. W., E. P. Maurer, A. Kumar, and D. P. Lettenmaier, 2002: Long-range experimental hydrologic forecasting for the eastern United States. *J. Geophys. Res.*, **107**, 4429, doi:10.1029/2001JD000659.

Xia, Y., and Coauthors, 2012: Continental-scale water and energy flux analysis and validation for the North American Land Data Assimilation System project phase 2 (NLDAS-2): 1. Intercomparison and application of model products. *J. Geophys. Res.*, **117**, D03109, doi:10.1029/2011JD016048.

Yuan, X., E. F. Wood, J. K. Roundy, and M. Pan, 2013: CFSv2-based seasonal hydroclimatic forecasts over the conterminous United States. *J. Climate*, **26**, 4828–4847, doi:10.1175/JCLI-D-12-00683.1.